ARO 30284.7-EG

ROBUST ALGORITHMS FOR PENETRATION MECHANICS PROBLEMS

FINAL REPORT

R.C. BATRA

October 1994

U.S. ARMY RESEARCH OFFICE

GRANT NO. DAAL03-92-G-0315

UNIVERSITY OF MISSOURI - ROLLA
ROLLA, MO 65401

REPORT DOCUMENTATION PAGE

Form Approved
OMB No. 0704-0188

1. AGENCY USE ONLY (Leave blank)	2. REPORT DATE	3. REPORT TYPE AND DATES COVERED
	October 1994	

4. TITLE AND SUBTITLE

Robust Algorithms for Penetration Mechanics Problems

5. FUNDING NUMBERS

DAAL03-92-G-0315

6. AUTHOR(S)

Romesh C. Batra

7. PERFORMING ORGANIZATION NAME(S) AND ADDRESS(ES)

University of Missouri-Rolla
Rolla, MO 65401-0249

8. PERFORMING ORGANIZATION REPORT NUMBER

9. SPONSORING/MONITORING AGENCY NAME(S) AND ADDRESS(ES)

U. S. Army Research Office
P. O. Box 12211
Research Triangle Park, NC 27709-2211

10. SPONSORING/MONITORING AGENCY REPORT NUMBER

ARO 30284.7-EG

11. SUPPLEMENTARY NOTES

The view, opinions and/or findings contained in this report are those of the author(s) and should not be construed as an official Department of the Army position, policy, or decision, unless so designated by other documentation.

12a. DISTRIBUTION/AVAILABILITY STATEMENT

Approved for public release; distribution unlimited.

12b. DISTRIBUTION CODE

13. ABSTRACT *(Maximum 200 words)*

We have studied the punching of a circular cylindrical hole in a steel plate impacted by a long rigid cylindrical rod. The material of the plate has been modeled by the Litonski-Batra constitutive relation, the effect of heat conduction is considered, the contacting surfaces are taken to be smooth, and the mesh is refined adaptively. Subsequent to the initial shock phase of impact during which the deformed plate material protrudes backwards, a plug ahead of the punch extrudes through the plate and a thin shear layer, characterized by the sharp transition of the axial velocity of plate particles, develops.

In an attempt to delineate the susceptibility of tungsten and depleted uranium penetrators to adiabatic shear banding, we have investigated the development of shear bands in a rectangular block of these materials deformed in plane strain compression at a nominal strain-rate of 5000/s. Deformations of a quarter of the domain are analyzed. The undeformed region is divided into 10^4 uniform rectangular elements and the yield strength of 300 randomly located elements is lowered by 5%. The numbers and orientations of shear bands are different in these two materials. The shear bands are found to initiate in tungsten at a lower value of the average strain than that in depeleted uranium.

14. SUBJECT TERMS	15. NUMBER OF PAGES
Axisymmetric Punch Problem, Shear Bands in Tungsten and Depleted Uranium.	50
	16. PRICE CODE

17. SECURITY CLASSIFICATION OF REPORT	18. SECURITY CLASSIFICATION OF THIS PAGE	19. SECURITY CLASSIFICATION OF ABSTRACT	20. LIMITATION OF ABSTRACT
UNCLASSIFIED	UNCLASSIFIED	UNCLASSIFIED	UL

NSN 7540-01-280-5500

Standard Form 298 (Rev. 2-89)
Prescribed by ANSI Std. Z39-18
298-102

TABLE OF CONTENTS

I. STATEMENT OF THE PROBLEM

The fundamental problem in penetration mechanics may be stated as (Wright and Frank[1]): Given a projectile, a target, and details of their initial geometry, kinematics, and materials; determine whether or not the target will be perforated upon impact. If perforated, find the residual characteristics of the projectile and the target, and if not, ascertain the shape and depth of the hole. Of the three approaches, namely, simple data correlation, engineering models, and numerical simulation used to analyze a penetration problem, we have concentrated on the third approach and developed robust and efficient algorithms capable of analyzing details of thermomechanical deformations of the penetrator and the target.

Factors that play a significant role during the penetration of metal targets by projectiles include material properties, impact velocity, projectile shape, target support position, and relative dimensions of the target and the projectile. Recently, emphasis has been placed on kinetic energy penetrators, which for terminal ballistic purposes may be considered as long metal rods traveling at high speeds. For impact velocities in the range of 2 to 10 km/sec, compressible hydrodynamic flow equations can be used to describe adequately the impact and penetration phenomena, because large stresses occurring in hypervelocity impact permit one to neglect the rigidity and compressibility of the striking bodies. Models, which require the use of the Bernoulli equation or its modification to describe this hypervelocity impact, have been proposed by Birkhoff *et al.*[2] and Pack and Evans.[3] At ordnance velocities (0.5 to 2 km/sec), material strength becomes an important parameter. Allen and Rogers[4] modified the Pack and Evans[3] flow model by representing the strength as a resistive pressure. This idea was taken further by Alekseevskii[5] and Tate,[6,7] who considered separate resistive pressures for the penetrator and the target. These resistive pressures are empirically determined quantities, and the predicted results depend strongly upon the assumed values of these pressures. As described lucidly by Wright[8] in his survey article on long rod penetrators, Tate's model is difficult to use for quantitative purposes, because the strength parameters depend upon the velocity of impact and the particular combination of materials involved.

The one-dimensional theories ignore the lateral motion, plastic flow, and the detailed dynamic effects. The paper by Backman and Goldsmith[9] is an authoritative review of the open literature on ballistic penetration, containing 278 reference citations from the 1800's to 1977. They describe different physical mechanisms involved in the penetration and perforation processes, and also discuss a number of engineering models. Jonas and Zukas[10] reviewed various analytical methods for the study of kinetic energy projectile-armor interaction at ordnance velocities and placed particular emphasis on three-dimensional numerical simulation of perforation. Anderson and Bodner[11] have recently reviewed engineering models for penetration and some of the major advances in hydrocode modeling of penetration problems. Three books,[12-14] published during the past few years, include extensive discussions of the engineering models, experimental techniques, and analytical modeling of ballistic perforation.

Manganello and Abbot,[15] Wingrove and Wulf,[16] and Recht[17] observed that the penetration resistance of some armor materials is reduced, even though these materials

mechanics formulated in either Lagrangian (HEMP) or Eulerian (HELP) coordinates. In the HEMP code, the finite difference operators are centered in space and time to give second order accuracy. The von Mises yield criterion and the incremental theory of plasticity are used to derive the incremental stress-strain relations. The material model employed in the HELP code includes the Tillotson equation of state modified to give a smooth transition between condensed and expanded states, the von Mises yield criterion with yield strength taken to increase with hydrostatic pressure and decrease linearly with the increase in the temperature, and a failure criterion based upon either a minimum value of the mass density or a critical value of the principal stress in tension.

Batra and Chen[35] recently developed a simple technique with which to analyze approximately the axisymmetric steady state deformations of a rigid/viscoplastic target being penetrated by a long rigid cylindrical rod with a hemispherical nose. They assume a kinematically admissible velocity field that satisfies the balance of mass, all of the essential boundary conditions, and traction boundary conditions on the axis of symmetry and on the target/penetrator interface, and they evaluate various parameters in the presumed velocity field by minimizing the error in the satisfaction of the balance of linear momentum. The computed results reveal that the leading term in the proposed velocity field gives a good solution that is reasonably close to the previously computed finite element solution of the problem. Batra and Gobinath[36] analyzed the steady state axisymmetric penetration problem for a deformable penetrator and target, and modeled the material for each as thermally softening, but strain and strain-rate hardening. They found that the bottom part of the target/penetrator interface is ellipsoidal rather than hemispherical. The peak pressures in the penetrator near the stagnation point approach $4.58\sigma_{op}$ and that in the target $14\sigma_{ot}$ when $\sigma_{op}/\sigma_{ot} = 3.06$. Here σ_{op} and σ_{ot} equal, respectively, the yield stress in a quasistatic simple compression test for the penetrator and target materials. The axial resisting force on the penetrator equaled 8.91 **F**, 11.52 **F**, and 14.51 **F** ($\mathbf{F} = \pi r_o^2 \sigma_{op}$) for stagnation point speeds of 450 m/s, 500 m/s, and 550 m/s, respectively. A significant contribution to the resisting force is made by the consideration of strain-rate hardening effects. When the penetrator and target materials are modeled as rigid/perfectly plastic, Gobinath and Batra[37] found that the resistive pressure terms in the modified Bernoulli's equation depend upon the ratio of the mass densities of the target and the penetrator as well as on the penetration speed.

The analysis of the steady state axisymmetric deformations of an elastic/perfectly plastic target being penetrated by a fast moving rigid cylindrical rod by Jayachandran and Batra[38] has revealed that the consideration of elastic effects reduces the value of the peak hydrostatic pressure acting at the stagnation point, the axial resisting force experienced by the penetrator, and the target resistance parameter appearing in the modified Bernoulli equation nearly 28%, 25%, and 25%, respectively. Batra and Jayachandran[39] modeled the thermoviscoplastic response of the target material by flow rules due to Litonski-Batra, Bodner-Partom,[40] and Brown, Kim, and Anand.[41] They calibrated the three flow rules against a hypothetical plane strain compression test performed at a nominal strain-rate of 3,300 sec^{-1} and then studied the axisymmetric penetration problem. They found that the three constitutive relations gave nearly the same value of the resisting force acting on the penetrator, temperature rise of material particles in the vicinity of the target/penetrator interface, and other macroscopic measures of deformation, such as the effective stress and

Fig. 2). This layer adjoins the surface of the hole punched in the plate and plastic deformations of the material within the layer are very intense. Even though the mesh has been refined adaptively, the scarcity of computational resources has limited our ability to decipher the width of the shear band.

In an attempt to understand the susceptibility of tungsten and depleted uranium penetrators to adiabatic shear banding, we have investigated the development of shear bands in a rectangular block of these materials deformed in plane strain compression at a nominal strain-rate of 5000/s. It is assumed that the deformations are symmetric about the horizontal and vertical centroidal axes; therefore, deformations of a quarter of the domain are studied. The undeformed region is divided into 10^4 uniform rectangular elements and it is assumed that the yield strength of 300 randomly located elements in the first quadrant is 5% lower than that of the remaining elements. In each case the material response is modeled by the Johnson-Cook relation with the values of material parameters taken from Rajendran's report.[46] As depicted in Figure 3, the pattern of shear bands formed in the two materials is quite different; similar patterns were obtained for 100 and 200 randomly located weak elements. In each case,[47] shear bands initiated in tungsten at a lower value of the average strain than that in depleted uranium. Batra, Zhang, and Wright[48] obtained a similar result for these two materials deformed in torsion which agrees with the experimental observations of Johnson *et al.*.[49]

We have incorporated the element erosion algorithm in conjunction with the Johnson-Cook model in DYNA2D. With this there is no need to refine the mesh adaptively since severely deformed elements are eliminated from the computations. Computations with identical depleted uranium and tungsten penetrators striking at normal incidence rolled homogeneous armor (RHA) steel plates reveal that the residual speed of depleted uranium penetrators is more than that of tungsten penetrators (*cf.* Fig. 4). This suggests that the depleted uranium penetrators should penetrate deeper into the thick target than identical tungsten penetrators.

We[50] have also proposed a four-stage engineering model of the penetration/perforation by hemispherical-nosed rigid cylindrical rods into targets whose material exhibits strain-hardening effects. During each stage of the penetration process, a kinematically admissible velocity field involving one or more unknown parameters is assumed. These parameters are determined by minimizing the rate of plastic dissipation from the velocity field, the incremental deformations of the target, the penetration depth, the resisting force acting on the penetrator and hence its deceleration are evaluated. A simple criterion for the formation and ejection of the cylindrical plug in the target has been proposed. Computed results (*cf.* Fig. 5) for the exit speed of the penetrator and when the targets are not perforated of the penetration depth are found to match well with the corresponding test values.

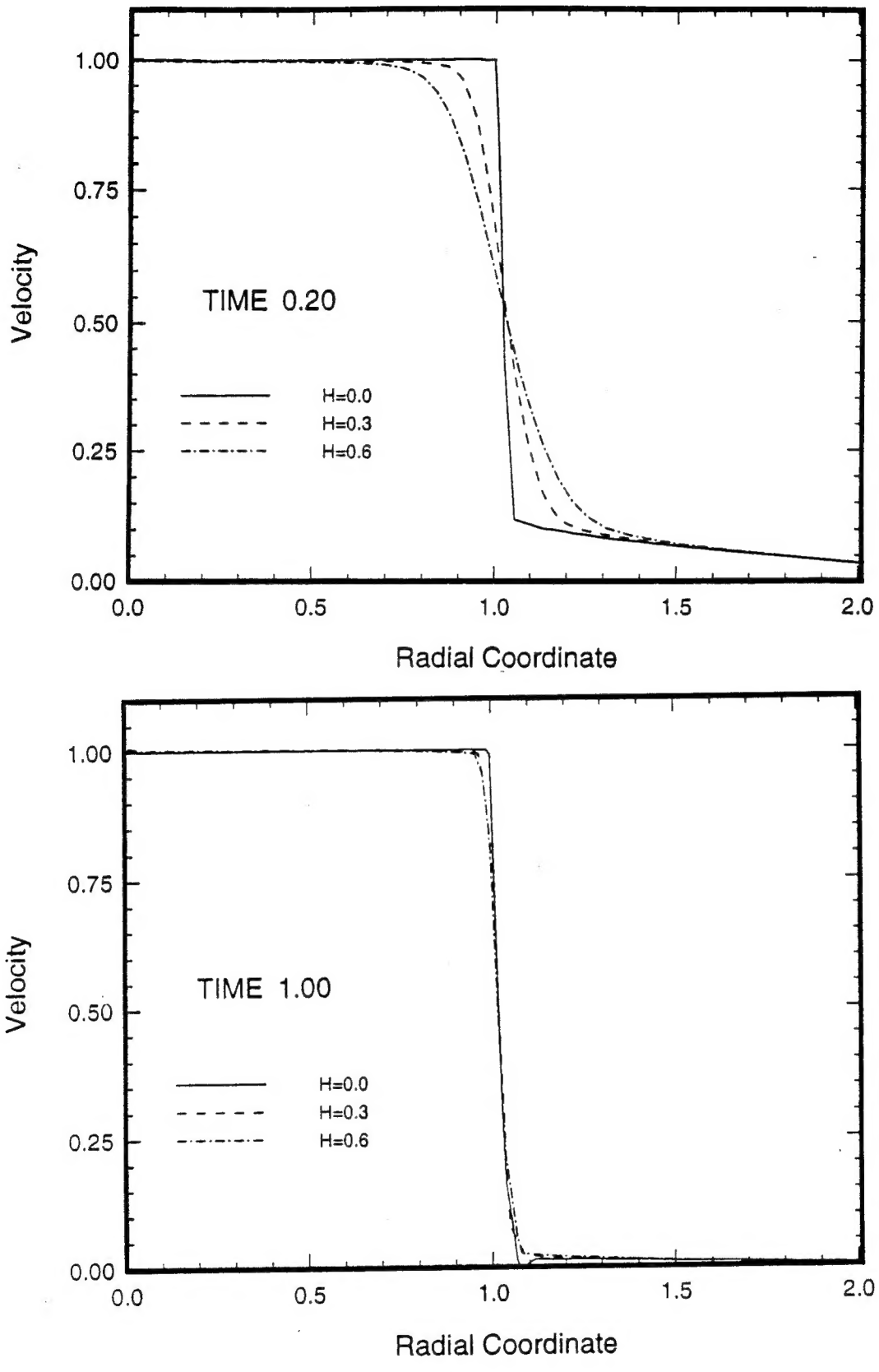

Fig. 2 Distribution of axial velocity on a horizontal line in the plate during its perforation by a rigid punch. The length is nondimensionalized with respect to the penetrator radius. H = distance from the punch face; the nondimensional time equals the nondimensional depth of the penetrator into the plate.

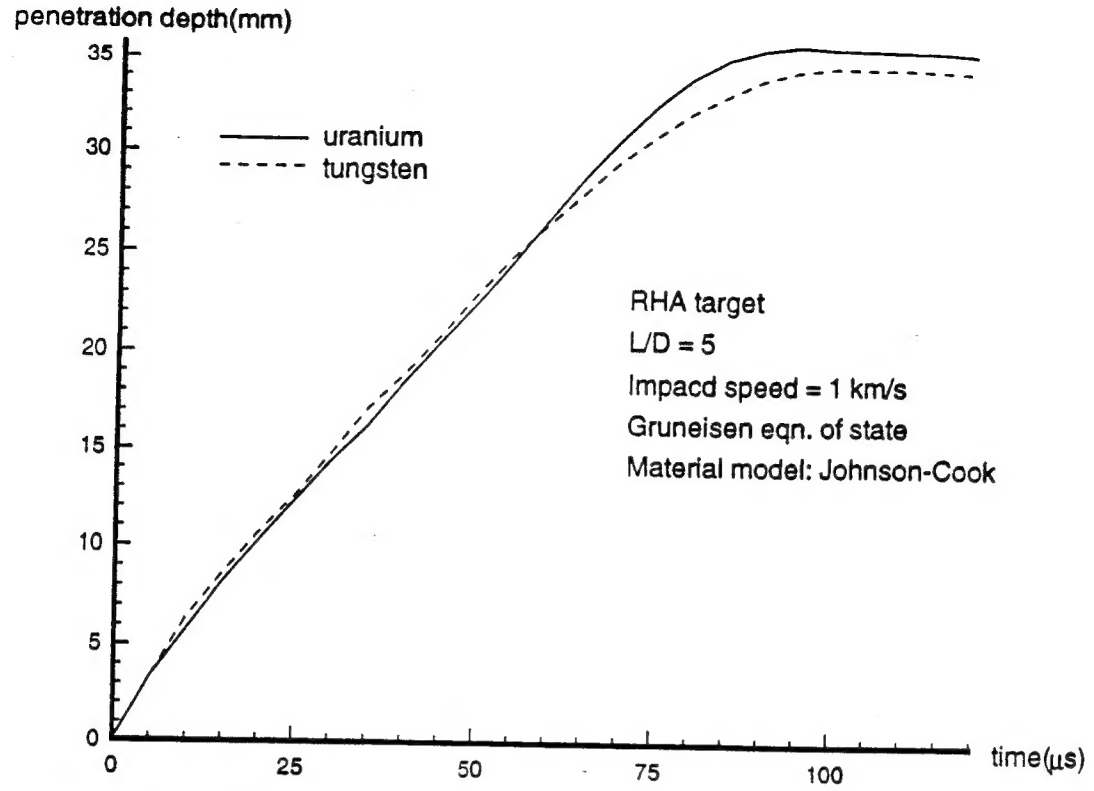

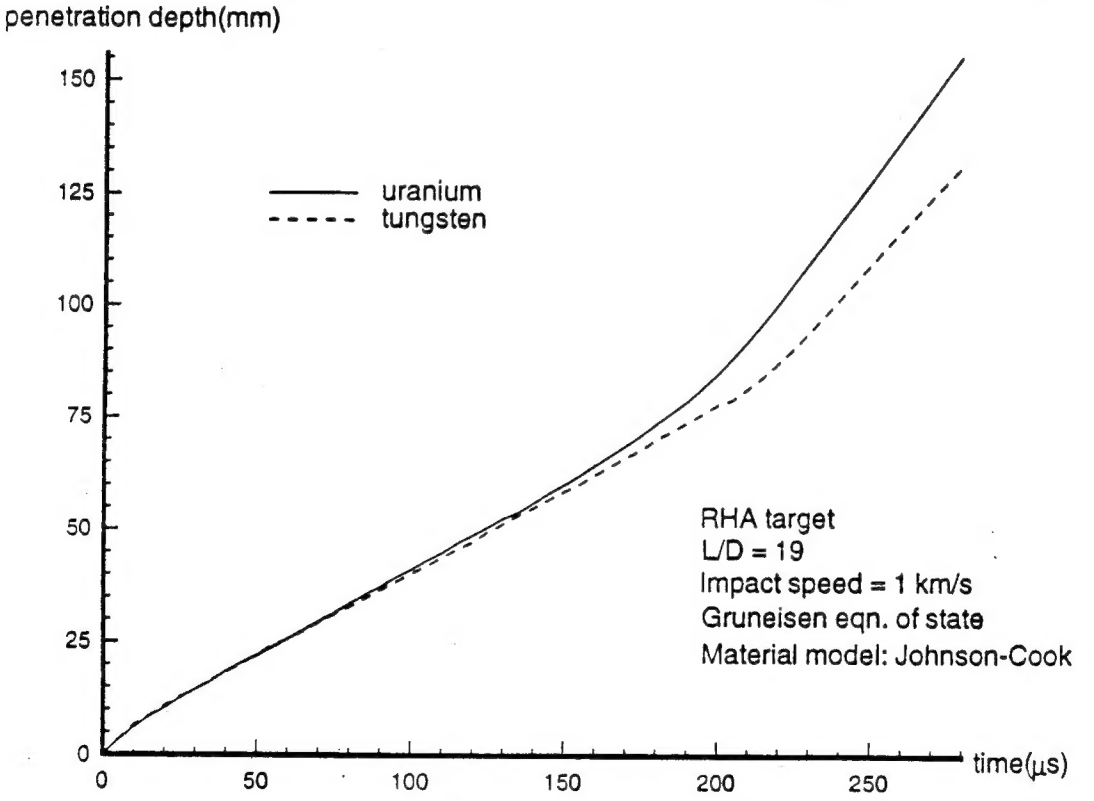

Fig. 4 Penetration depth vs. time for depleted uranium and tungsten rods striking at normal incidence RHA steel plates.

III. LIST OF PUBLICATIONS:

1. R.C. Batra and R. Jayachandran, Steady State Axisymmetric Penetration of a Kinematically Hardening Thermoviscoplastic Target, *Int. J. Engr. Sci.*, 31, 1309-1323, 1993.

2. Xingju Chen and R.C. Batra, Axisymmetric Penetration of Thick Thermoviscoplastic Targets, *Proc. Symp. on Advances in Numerical Simulation Techniques for Perforation and Penetration of Solids*, (E.P. Chen and V.K. Luk, eds.), ASME-AMD Vol. 171, pp. 125-132, 1993.

3. R.C. Batra and X. Chen, Effect of Frictional Force and Nose Shape on Axisymmetric Deformations of a Thick Thermoviscoplastic Target, *Acta Mechanica*, Vol. 106, pp. 87-105, 1994.

4. Xingju Chen and R.C. Batra, Deep Penetration of Thick Thermoviscoplastic Targets by Long Rigid Rods, *Computers and Structures*, (in press).

5. X. Chen, Finite Element Analysis of Axisymmetric Deformations of Thick Thermoviscoplastic Targets, Ph.D. Dissertation, Univ. of Missouri-Rolla, 1993.

6. Y. Wu and R.C. Batra, An Engineering Penetration/Perforation Model of Hemispherical Nosed Rigid Cylinderical Rods into Strain-Hardening Targets, *Computers & Structures*, (in press).

7. R.C. Batra, X. Chen, Z. Peng and Y. Wu, On Axisymmetric Penetration/Perforation of Thermoviscoplastic Targets, *Proc. IUTAM Symp. on Impact Dynamics*, Beijing, China, (in press).

8. R.C. Batra and Z. Peng, Development of Shear Bands in Dynamic Plane Strain Compression of Depleted Uranium and Tungsten Blocks, *Int. J. Impact Eng'g.* (in press).

LIST OF PRESENTATIONS:

1. X. Chen and R.C. Batra, Axisymmetric Penetration of Thick Thermoviscoplastic Targets, *1st Joint SES/ASME/ASCE Meeting*, Univ. of Virginia, Charlottesville, VA, June 6-9, 1993.

2. R.C. Batra and X. Chen, Effect of Thermal Softening on the Penetration of a Steel Rod into an Aluminum Target, *4th Int. Symp. on Plasticity and Its Current Applications*, Baltimore, MD, July 1993.

3. R.C. Batra, X.J. Chen, and Z. Peng, Axisymmetric Penetration of Thermoviscoplastic Targets, *Army Symp. on Solid Mechanics*, Plymouth, MA, August 1993.

4. R.C. Batra, On Axisymmetric Penetration of Thick Thermoviscoplastic Targets, *Symp.*

BIBLIOGRAPHY

1. T.W. Wright and K. Frank, Approaches to Penetration Mechanics, in Impact: Effects of Fast Transient Loading (W.J. Ammann, W.K. Liu, J.A. Studer, and T. Zimmerman, Eds.), A.A. Balkema, Rotterdam, 1988.

2. G. Birkhoff, D.P McDougall, E.M. Pugh, and G. Taylor, *Proc. Phys. Soc. Lond.* **57** 147 (1945).

3. D.C. Pack and W.M. Evans, *Proc. Phys. Soc. Lond.* **B64** 298 (1951).

4. W.A. Allen and J.W. Rogers, *J. Franklin Ins.* **272** 275 (1961).

5. V.P. Alekseevskii, *Combst. Explo. Shock Waves*, **2** 63 (1966).

6. A. Tate, *J. Mech. Phys. Sol.*, **15** 387 (1967).

7. A. Tate, *J. Mech. Phys. Sol.*, **17** 141 (1969).

8. T.W. Wright, A Survey of Penetration Mechanics for Long Rods, in Lecture Notes in Engineering, v. 3, Computational Aspects of Penetration Mechanics, J. Chandra and J. Flaherty, eds., Springer-Verlag, New York, 1984.

9. M.E. Backman and W. Goldsmith, *Int. J. Eng. Sci.*, **16** 1 (1978).

10. G.H. Jonas and J.A. Zukas, *Int. J. Eng. Sci.*, **16** 879 (1978).

11. C.E. Anderson and S.R. Bodner, The Status of Ballistic Impact Modeling, Proc. 3rd TACOM Armor Coordinating Conf., Feb. 17-19, 1987, Monterey, CA.

12. J.A. Zukas (ed.), High Velocity Impact Dynamics, John Wiley & Sons, Inc., New York, 1990.

13. E.W. Billington and A. Tate, The Physics of Deformation and Flow, McGraw-Hill, New York (1981).

14. J.A. Zukas, T. Nicholas, H.F. Swift, L.B. Greszczuk, and D.R. Curran, Impact Dynamics, John Wiley, New York (1982).

15. S.J. Manganello and K.H. Abbott, *J. Mats.*, **7** 231 (1972).

16. A.L. Wingrove and G.L. Wulf, *J. Aust. Inst. Met.*, **18** 167 (1973).

17. R.F. Recht, I. Mech. E., 3rd Int. Conf. on High Pressure, Scotland (May 1970).

18. T.A.C. Stock and K.R.L. Thompson, *Met. Trans.*, **1** 219 (1970).

19. A.J. Bedford, A.L. Wingrove, and K.R.L. Thompson, *J. Aust. Inst. Met.*, **19** 61 (1974).

42. R.C. Batra and A. Adam, *Int. J. Engng. Sci.*, 29 1391 (1991).

43. R.C. Batra and A. Adam, *Computers and Structures*, **42** 489 (1992).

44. X. Chen and R.C. Batra, *Acta Mechanica*, **106**, 87, 1994.

45. M.J. Forrestal, N.S. Brar and V.K. Luk, *J. Appl. Mech.*, **58**, 7 (1991).

46. A.M. Rajendran, High Strain Rate Behavior of Metals, Ceramics, and Concrete, Report #WL-TR-92-4006, Wright Patterson Air Force Base (1992).

47. R.C. Batra and Z. Peng, Development of Shear Bands in Dynamic Plane Strain Compression of Depleted Uranium and Tungsten Blocks, *Int. J. Impact Engng.*, (in press)

48. R.C. Batra, X.T. Zhang and T.W. Wright, Critical Strain Ranking of Twelve Materials in Deformations Involving Adiabatic Shear Bands, *J. Appl. Mechs.* (in press)

49. G.R. Johnson, J.M. Hoegfeldt, U.S. Lindholm and A. Nagy, *ASME J. Eng'g Mat. & Technology*, **105**, 48 (1983).

50. Y. Wu and R.C. Batra, An Engineering Penetration/Perforation Model of Hemispherical Nosed Rigid Cylindrical Rods into Strain-Hardening Targets, *Computers & Structures*, (in press).

Int. J. Engng Sci. Vol. 31 No. 9, pp. 1309–1323, 1993
Printed in Great Britain.

0020-7225/93 $6.00 + 0.00

STEADY STATE AXISYMMETRIC PENETRATION OF A KINEMATICALLY HARDENING THERMOVISCOPLASTIC TARGET

R. C. BATRA

Department of Mechanical and Aerospace Engineering and Engineering Mechanics, University of Missouri–Rolla, Rolla, MO 65401-0249, U.S.A.

R. JAYACHANDRAN

Department of Mechanical Engineering, Massachusetts Institute of Technology, Cambridge, MA 02139, U.S.A.

Abstract—We study axisymmetric thermomechanical deformations of a thick target being penetrated by a fast-moving rigid cylindrical rod with a hemispherical nose, and presume that target deformations appear steady to an observer situated at the penetrator nose tip. Both isotropic and kinematic hardening of the target material are considered. It is found that kinematic hardening increases the normal stress acting on the penetrator nose surface and the temperature rise of target particles abutting the penetrator. However, the value of the hydrostatic pressure at a point in the deforming target region is affected very little by the consideration of kinematic hardening. For suitable values of material parameters appearing in the evolution equation of the back-stress, the computed values of the back-stress at target particles abutting the penetrator nose surface equal three times the yield stress of the target material in a quasistatic simple compression test.

1. INTRODUCTION

During the penetration of a thick target by a fast-moving cylindrical rod, target and penetrator material particles in the vicinity of the target/penetrator interface are deformed severely, and are also heated up significantly. Consequently, the material undergoes microstructural changes such as the generation/annihilation of dislocations, dynamic recovery and recrystallization, development of texture, nucleation and growth of microcracks and voids, and possibly the development of shear bands that form during the intense plastic deformations of a material, especially at high strain rates. One way to account for these microstructural changes is to use constitutive equations which employ a suitable number of scalar and tensor valued internal variables (e.g. see Coleman and Gurtin [1], Chan *et al.* [2], Inoue [3], Lubliner [4], and Anand [5]). Here we use one scalar variable to describe the isotropic hardening, and a traceless symmetric second-order tensor, also known as the back stress tensor, to account for the kinematic hardening of the material. The Litonski–Batra constitutive relation (e.g. see Batra and Jayachandran [6]) is modified to incorporate the kinematic hardening and used herein to study the thermomechanical axisymmetric deformations of the target. The hemispherical nosed cylindrical penetrator is assumed to be rigid and the target deformations steady, as seen by an observer situated at the penetrator nose tip and moving with it. We note that Batra and Jayachandran [6] recently analyzed thermomechanical deformations of a target by using three constitutive relations, namely, those due to Litonski–Batra, Bodner–Partom [7], and Brown *et al.* [8]. Each of these was calibrated to give almost identical effective stress vs logarithmic strain curves for a block made of target material and deformed in plane strain compression at an average strain-rate of $3300\,s^{-1}$. Even though these constitutive relations account for the evolution of the microstructural changes in different ways, they gave essentially identical results for the resisting force experienced by the penetrator, normal stress on the penetrator nose surface, and the distribution of the tangential speed and the second-invariant of the strain-rate tensor on the penetrator nose surface.

This work is in the spirit of the one initiated by Batra and Wright [9], and is aimed at providing guidelines for selecting and improving upon the previously used kinematically

Here $\mathbf{v}$ is the velocity of a material particle, $\boldsymbol{\sigma}$ the Cauchy stress tensor at the present location of a material particle, ρ the mass density, $\mathbf{q}$ the heat flux, $\mathbf{D}$ the stretching tensor, and $\mathbf{W}$ the spin tensor. The balance laws (1), (2), and (3) are written in the Eulerian description of motion, and the operators grad and div denote the gradient and divergence operators on fields defined in the present configuration. Equation (1) implies that both the elastic and plastic deformations of the target are assumed to be isochoric. Equation (5) is the Fourier law of heat conduction with k the thermal conductivity and θ the temperature rise of a material particle. Equation (6) is the presumed constitutive relation for the specific internal energy U, wherein c is the specific heat. In equations (7)–(13), $\boldsymbol{\sigma}$ is the Cauchy stress tensor, $\mathbf{s}$ its deviatoric part, p the hydrostatic pressure not determined by the deformation history, $\mathbf{B}$ the traceless symmetric second-order tensor used to account for the kinematic hardening of the material, and ψ is a scalar internal variable that accounts for the isotropic hardening of the material. The evolution equation (10) for $\mathbf{B}$ has been proposed by White *et al.* [43]. Equation (9) with μ given by equation (11) is a generalization of the Litonski–Batra law to account for the kinematic hardening of the material. Here σ_0 is the yield stress in a quasistatic simple tension or compression test, parameters b and m characterize the strain-rate sensitivity of the material, v its thermal softening, and b its workhardening. In a quasistatic simple tension or compression test,

$$\sigma = \sigma_0\left(1 + \frac{\psi}{\psi_0}\right)^n$$

describes the stress–strain curve, where ψ is now interpreted as the plastic strain. In a dynamic test, the effect of the history of deformation upon the present state of deformation is accounted for through the parameter ψ.

We nondimensionalize variables by scaling stress-like quantities by σ_0, length by r_0, time by (r_0/v_0), and the temperature by the reference temperature θ_r, defined by

$$\theta_r \equiv \sigma_0/\rho c. \tag{14}$$

Here r_0 equals the radius of the cylindrical part of the penetrator and v_0 the penetration speed. In terms of nondimensional variables, the aforestated governing equations become

$$\operatorname{div}\mathbf{v} = 0, \tag{15.1}$$

$$-\operatorname{grad} p + \operatorname{div}\mathbf{s} = \alpha(\mathbf{v}\cdot\operatorname{grad})\mathbf{v}, \tag{15.2}$$

$$\mathbf{s} - \mathbf{B} + \beta\gamma((\mathbf{v}\cdot\operatorname{grad})\mathbf{s} + \mathbf{sW} - \mathbf{Ws}) = 2\beta\mathbf{D}, \tag{15.3}$$

$$\operatorname{tr}(\boldsymbol{\sigma}\mathbf{D}^p) + \delta\operatorname{div}(\operatorname{grad}\theta) = (\mathbf{v}\cdot\operatorname{grad})\theta, \tag{15.4}$$

$$(\mathbf{v}\cdot\operatorname{grad})\mathbf{B} + \mathbf{BW} - \mathbf{WB} + \xi_2 I\mathbf{B} = \xi_1\mathbf{D}^p, \tag{15.5}$$

$$(\mathbf{v}\cdot\operatorname{grad})\psi = \operatorname{tr}(\boldsymbol{\sigma}\mathbf{D}^p)\Big/\left(1 + \frac{\psi}{\psi_0}\right)^n, \tag{15.6}$$

where

$$\alpha = \frac{\rho v_0^2}{\sigma_0}, \qquad \beta = \frac{\mu v_0}{\sigma_0 r_0}, \qquad \gamma = \frac{\sigma_0}{G}, \quad \text{and} \quad \delta = \frac{k}{\rho c v_0 r_0} \tag{15.7}$$

are nondimensional numbers. Henceforth, we will use nondimensional variables only. For a given problem, α, γ, and δ are constants, but β varies from point to point in the deforming region because of the variation in μ. The value of α signifies the importance of inertia forces relative to the flow stress of the material, and may be thought of as the reciprocal of the Reynolds number in a viscous fluid. The values of γ and δ give the effect of material elasticity and heat conduction, respectively. For typical penetration problems involving long rod penetrators, δ is of the order of 10^{-5}; hence target deformations may be considered adiabatic.

$$\sigma_{zz}=0, \quad v_r=0, \quad \frac{\partial\theta}{\partial z}=0 \quad \text{on the surface AB,} \tag{16.4}$$

$$v_r=0, \quad v_z=-1, \quad \theta=0, \quad \psi=0, \quad p=0, \quad s_{rr}=0, \quad s_{\theta\theta}=0, \quad s_{zz}=0,$$
$$s_{rz}=0, \quad B_{rr}=0, \quad B_{\theta\theta}=0, \quad B_{zz}=0, \quad B_{rz}=0 \quad \text{on the bounding surface EFA,} \tag{16.5}$$

$$\sigma_{rz}=0, \quad v_r=0, \quad \frac{\partial\theta}{\partial r}=0 \quad \text{on the axis of symmetry DE.} \tag{16.6}$$

Here $\mathbf{n}$ and $\mathbf{t}$ denote, respectively, a unit normal and a unit tangent vector to the surface, θ_a is an average temperature of the penetrator, h_c is the heat transfer coefficient between the penetrator and the target, and Γ_i denotes the target/penetrator interface. The boundary conditions (16) incorporate the assumptions that Γ_i is smooth, there is no interpenetration of the target material into the penetrator and vice versa, the deformations are axisymmetric, and the bounding surfaces AB and EFA are far removed from the penetrator nose surface. The boundary conditions (16.5) on p and components of $\mathbf{s}$ and $\mathbf{B}$ on the surface EFA are needed, since we solve equations (15.3) and (15.5) for $\mathbf{s}$ and $\mathbf{B}$, along with the other equations for p, $\mathbf{v}$, θ, and ψ; e.g. see Shimazaki and Thompson [44].

We refer the reader to [10] for details of obtaining a finite element solution of the problem, and ensuring that the region R studied herein is adequate. The computer code used to analyze the thermomechanical problem discussed in [6] was modified to include the effect of kinematic hardening.

3. NUMERICAL RESULTS

In an attempt to study the effect of kinematic hardening on the solution variables, the values of material parameters ξ_1 and ξ_2 in equation (15.5) were varied over a wide range. However, the other material and geometric parameters were assigned the following values, taken from [6], for an HY-100 steel.

$$\rho=7860\ \text{kg/m}^3, \quad \sigma_0=405\ \text{MPa}, \quad G=80\ \text{GPa}, \quad c=473\ \text{J/kg°C},$$
$$k=50\ \text{W/m°C}, \quad h=20\ \text{W/m}^2\text{°C}, \quad \theta_a=0, \quad r_0=10\ \text{mm}, \quad b=10\ \text{s},$$
$$\nu=1.2\times10^{-3}/\text{°C}, \quad \psi_0=0.1, \quad m=0.01, \quad n=0.13, \quad \alpha=2.0. \tag{17}$$

Thus, the reference temperature used to nondimensionalize the temperature rise equals 108.9°C.

Wang and Batra [45] have recently studied the initiation and growth of shear bands in a thermally softening viscoplasitc block obeying constitutive relations similar to equations (8)–(12) and deformed in plane strain compression at an average strain-rate of $5000\ \text{s}^{-1}$. Their load-displacement curves (cf. Fig. 10 of [45]) for the homogeneous block show that an increase in the value of ξ_1 hardens the material and an increase in the value of ξ_2 softens it in the sense that the load required to compress the block by a certain amount is more for higher values of ξ_1 and less for larger values of ξ_2. Earlier computations by Batra and Jayachandran [6] and Jayachandran and Batra [19] suggest that a change in the values of ξ_1 and ξ_2 should affect the deformations of the target in an analogous manner.

All of the results presented below and values of variables indicated in figures, unless stated otherwise, are nondimensional.

3.1 Results with ξ_2 varied

Figure 2 depicts the distribution of the normal stress, temperature rise, tangential speed, and the second invariant of the strain-rate tensor, also referred to as the strain-rate measure, on the

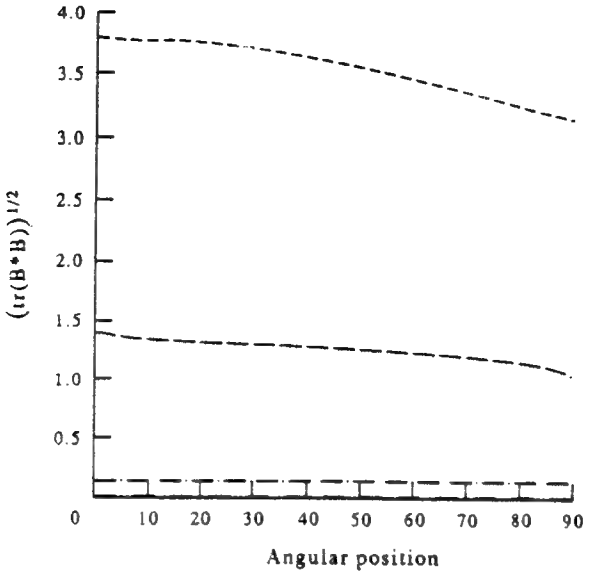

Fig. 3. Distribution of $(\mathrm{tr}(\mathbf{B}\,\mathbf{B}^{\mathrm{r}}))^{1/2}$ upon the penetrator nose surface for $\xi_1 = 1.0$ and four different values of ξ_2. See Fig. 2 for the legend to curves. The curve for $\xi_2 = 100$ essentially coincides with the horizontal axis.

for the hemispherical nose surface was found to equal 7.87 for the case of no kinematic hardening, and 9.61, 8.57, 7.86, and 7.77 for $\xi_2 = 0$, 1, 10, and 100, respectively. The dimensional values of F are obtained by multiplying the nondimensional ones by $\pi r_0^2 \sigma_0$. Note that in our work the speed of penetration is kept fixed, and whatever additional energy is required for the penetration process is presumed to be available. The noticeable increase in the temperature rise for $\xi_2 = 0$, 1, and 10 is due to the significant values of $\mathbf{B}$, see Fig. 3, and the observation, verified by the computed results that $\mathrm{tr}(\mathbf{B}\mathbf{D}^p) \geq 0$. Since values of $(\mathbf{s} - \mathbf{B})$ affect the plastic deformations of the material, an increase in the value of $\mathbf{B}$ will necessitate higher values of $\mathbf{s}$, which will cause more plastic working and, hence, greater temperature rise. The variation of the strain-rate measure, axial stress, temperature rise, and the axial velocity on the central line plotted in Fig. 4 reveals that the consideration of kinematic hardening affects these variables at points situated at most one penetrator radius from the penetrator nose tip.

An integration of equation (15.2) along the central streamline ($r = 0$) gives

$$\frac{1}{2}\alpha v^2 + p - s_{zz} - 2\int_0^z \frac{\partial \sigma_{rr}}{\partial r}\,\mathrm{d}z = -\sigma_{zz}(0). \tag{19}$$

Setting $z = 0$ and comparing the result with Tate's equation [33, 34], we get

$$R_t = -\sigma_{zz}^s - \frac{\alpha}{2} \tag{20}$$

where R_t equals the strength parameter for the target in Tate's equation, and σ_{zz}^s is the value of σ_{zz} at the stagnation point. The computed values of R_t for $\xi_2 = 0$, 1, 10, and 100 were found to be 10.63, 8.91, 8.05, and 7.97, respectively. For the case of no kinematic hardening, $R_t = 8.01$. According to Tate [33, 34],

$$R_t = \frac{2}{3} + \ln\left(\frac{2}{3}\frac{E}{\sigma_0}\right) \tag{21}$$

where E equals Young's modulus for the target material. Thus, Tate's formula gives $R_t = 6.64$. We note that for $\xi_2 = 0$ and 1, the values of s_{zz}^s were higher than those for $\xi_2 = 10$ and 100. Since the plastic deformation is governed by $(s_{zz} - B_{zz})$, higher values of B_{zz} necessitate a corresponding increase in the values of s_{zz}. For $\xi_2 = 0$, 1, 10, and 100, the values of $-s_{zz}(0)$

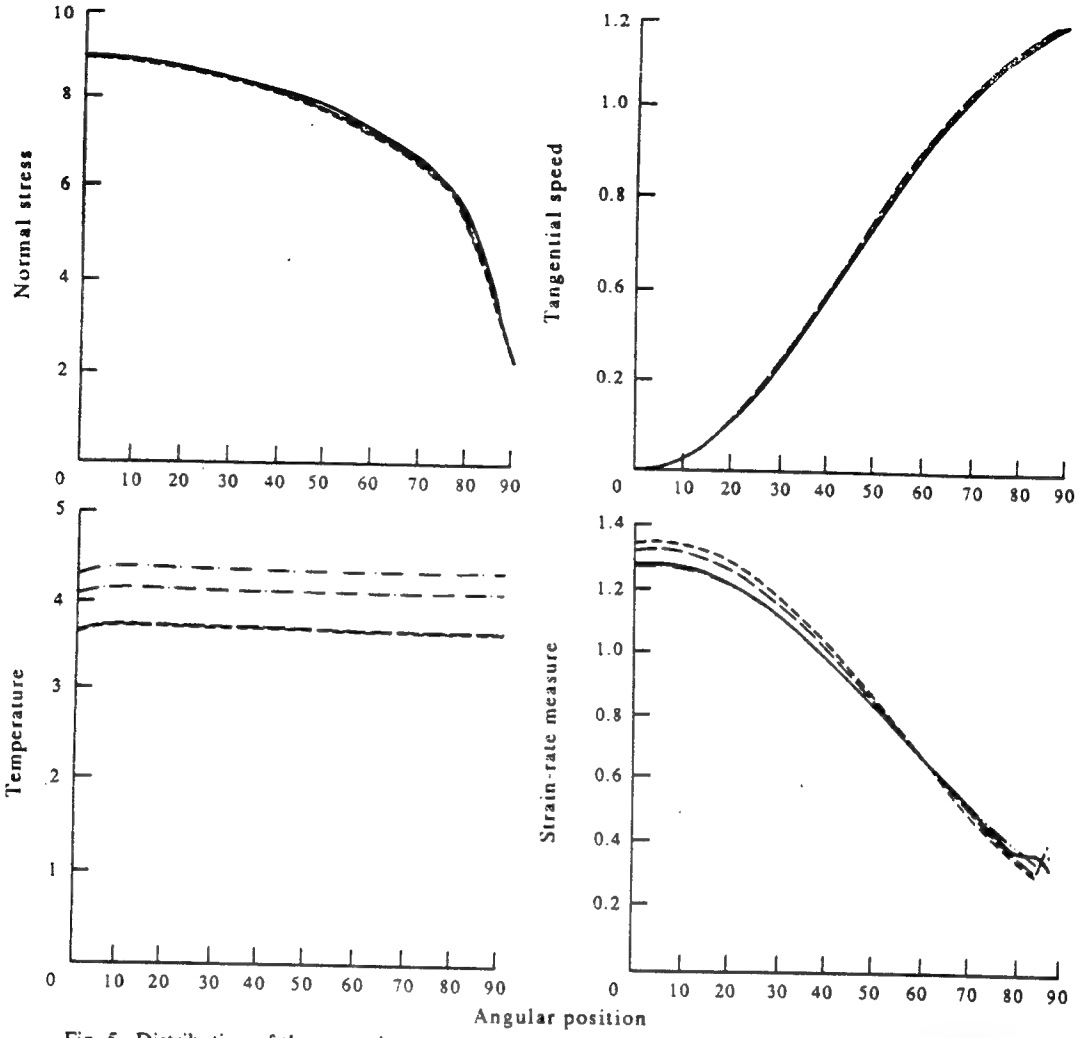

Fig. 5. Distribution of the normal stress, tangential speed, temperature rise, and the second invariant of the strain-rate tensor on the hemispherical nose surface of the penetrator for $\xi_1 = 10^4$ and four different values of ξ_2. —— no kinematic hardening; – – – $\xi_2 = 10^8$; ----- $\xi_2 = 10^6$; – · – $\xi_2 = 10^5$; – · · – $\xi_2 = 6.5 \times 10^4$.

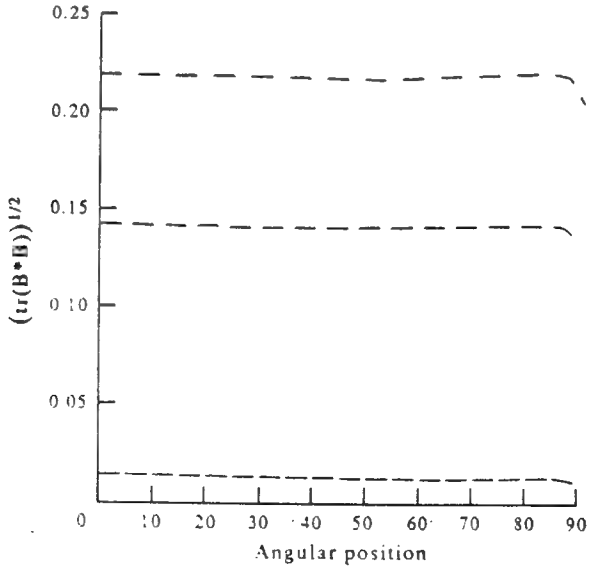

Fig. 6. Distribution of $(\mathrm{tr}(\mathbf{B}\,\mathbf{B}^{\mathrm{T}}))^{1/2}$ upon the penetrator nose surface for $\xi_1 = 10^4$ and four different values of ξ_2. See Fig. 5 for the legend to curves. The curve for $\xi_2 = 10^8$ coincides with the horizontal axis.

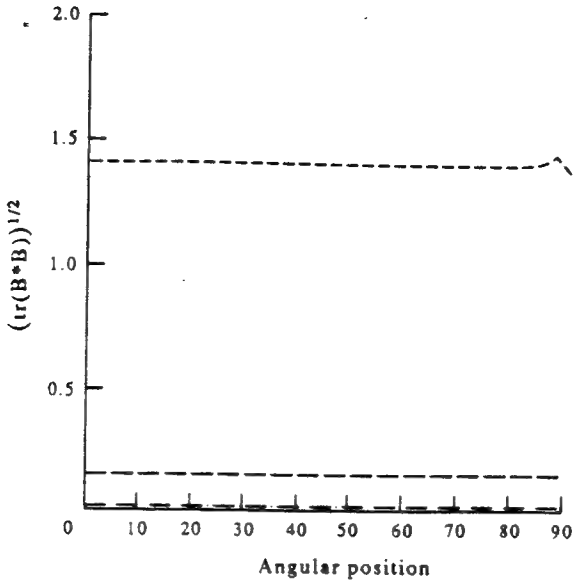

Fig. 8. Distribution of $(\mathrm{tr}(\mathbf{B}\,\mathbf{B}^{\mathrm{T}}))^{1/2}$ upon the penetrator nose surface for $\xi_2 = 100$ and four different values of ξ_1. See Fig. 7 for the legend to curves. The curve for $\xi_1 = 0.1$ coincides with the horizontal axis.

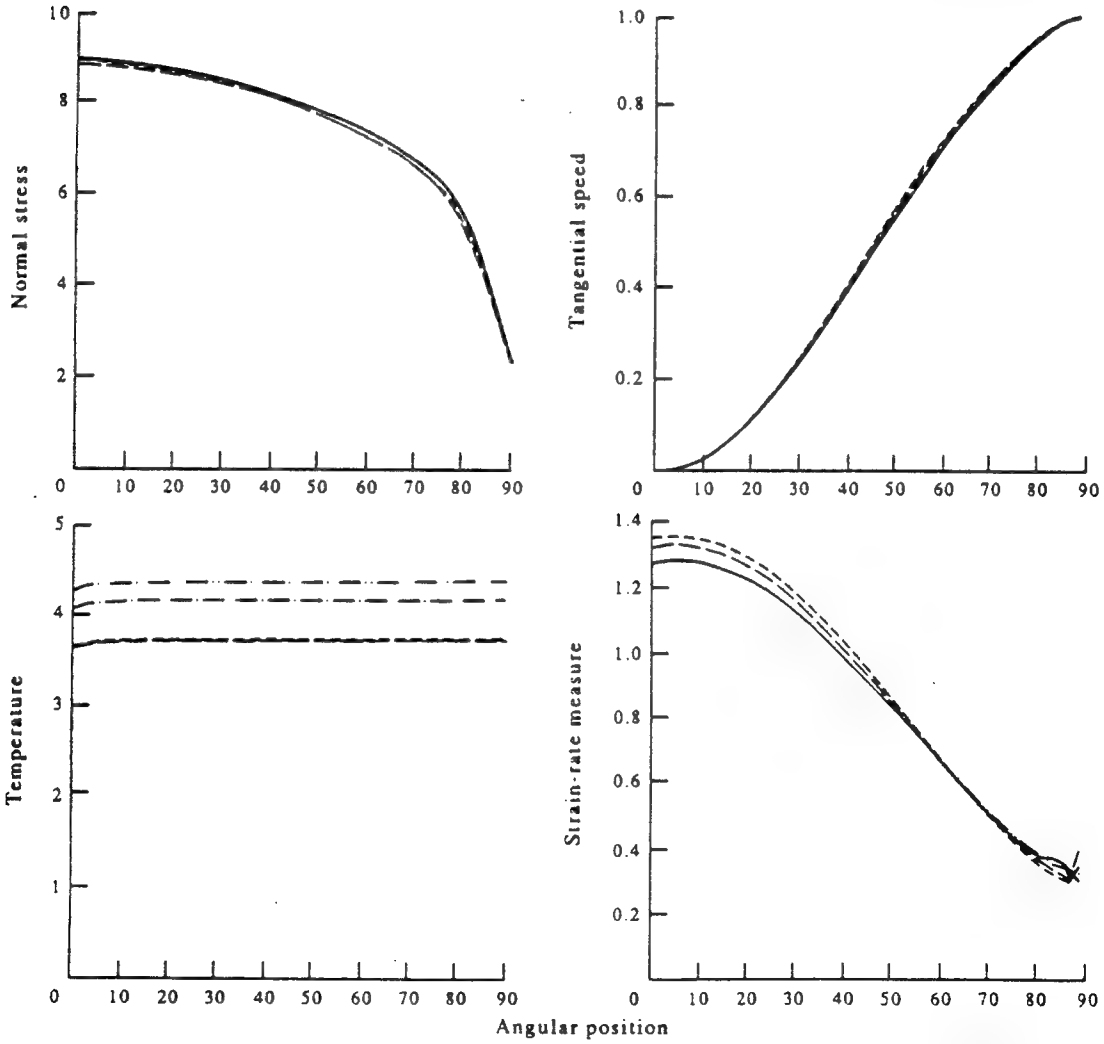

Fig. 9. Distribution of the normal stress, tangential speed, temperature rise, and the second invariant of the strain-rate tensor on the hemispherical nose surface of the penetrator for $\xi_2 = 10^6$ and four different values of ξ_1. —— no kinematic hardening; – – – $\xi_1 = 10^2$; ----- $\xi_1 = 10^4$; – · – $\xi_1 = 10^5$; – · · – $\xi_1 = 1.5 \times 10^5$.

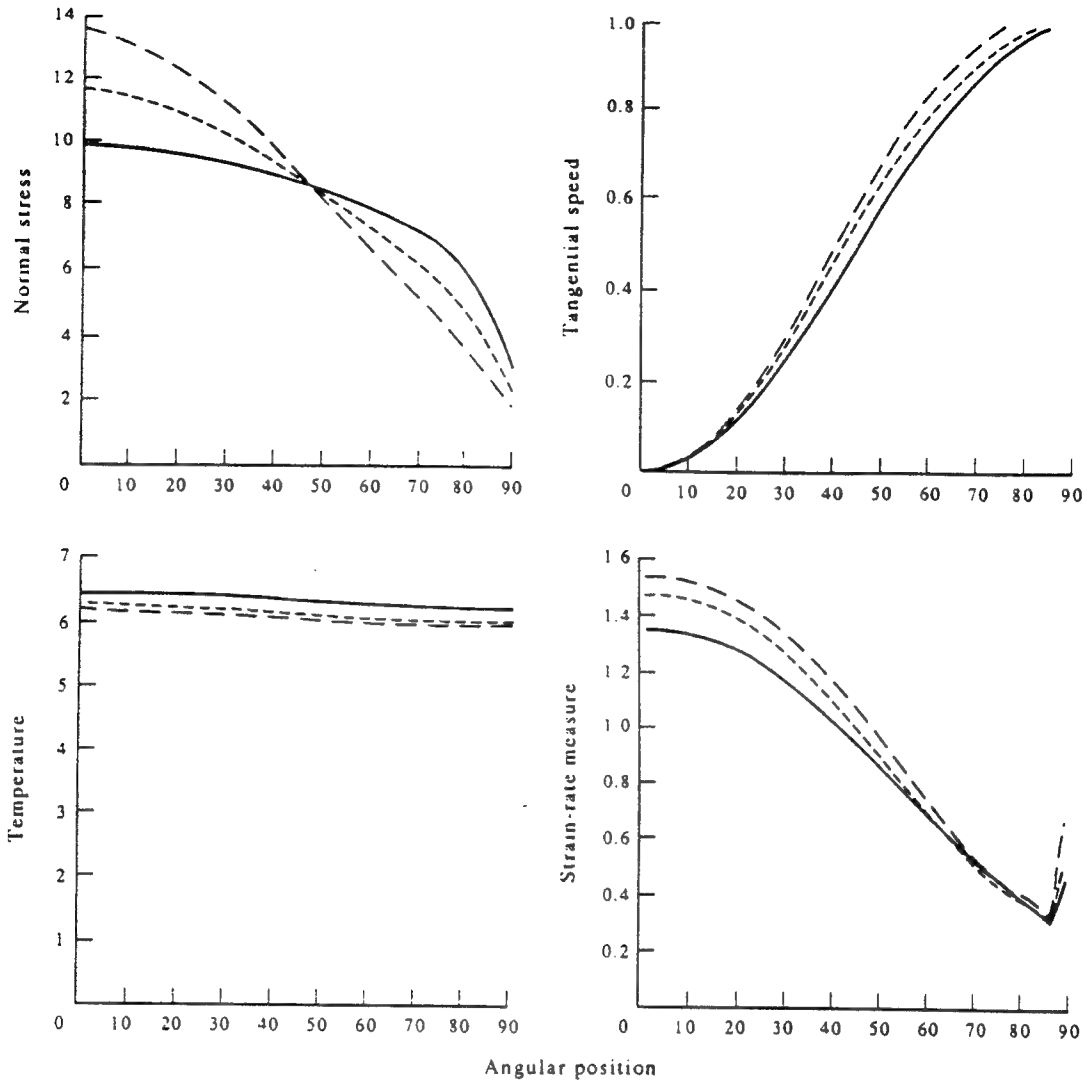

Fig. 11. Distribution of the normal stress, tangential speed, temperature rise, and the second invariant of the strain-rate tensor on the hemispherical nose surface of the penetrator for $\xi_1 = 1$, $\xi_2 = 100$, and three different values of α; —— $\alpha = 2$; ----- $\alpha = 6$; and – – – $\alpha = 10$.

from the crater surface, and then quite slowly. The contours of I_B for other values of ξ_1 and ξ_2 are similar to those shown in Fig. 10 and are not included herein.

3.3 Results with α varied

We have plotted in Fig. 11 the distribution on the penetrator nose surface of the normal stress, temperature rise, tangential speed, and the strain-rate measure for $\alpha = 2$, 6, and 10 with $\xi_1 = 1$ and $\xi_2 = 100$ kept fixed. The normal stress distribution on the penetrator nose surface resembles that computed by Batra and Wright [9] for the case of no kinematic hardening in the sense that its value at the point for which $\psi \approx 46°$ is unaffected by the value of α, and it increases with α for $\psi < 46°$ and decreases with α for $\psi > 46°$. We note that Batra and Wright used a coarse finite element mesh consisting of 6-noded triangular elements and considered a smaller target region than that studied herein. The values of the strain-rate measure increase with α for $\psi < 60°$, those of the tangential speed increase with α for $10° \le \alpha \le 80°$, and the temperature distribution on the penetrator nose surface is affected very little when α is increased from two to ten. The distribution of $(\mathrm{tr}(\mathbf{B}\,\mathbf{B}^{\mathrm{T}}))^{1/2}$ on the penetrator nose surface,

[7] S. R. BODNER and Y. PARTOM, *J. appl. Mech.* **42,** 385 (1975).
[8] S. B. BROWN, K. H. KIM and L. ANAND, *Int. J. Plasticity*, **5,** 95 (1989).
[9] R. C. BATRA and T. W. WRIGHT, *Int. J. Engng Sci.* **24,** 41 (1986).
[10] R. JAYACHANDRAN and R. C. BATRA, *Acta mech.* **92,** 9 (1992).
[11] R. C. BATRA and T. GOBINATH, *Int. J. Impact Engng.* **11,** 1 (1991).
[12] T. GOBINATH and R. C. BATRA, *Int. J. Engng Sci.* **29,** 1315 (1991).
[13] R. C. BATRA, *Int. J. Engng Sci.* **25,** 1131 (1987).
[14] R. C. BATRA, *Comp. Mech.* **3,** 1 (1988).
[15] R. C. BATRA and P.-R. LIN, *Int. J. Engng Sci.* **26,** 183 (1988).
[16] R. C. BATRA and P. R. LIN, *Int. J. Impact Engng.* **8,** 99 (1989).
[17] R. C. BATRA and P. R. LIN, *Int. J. Engng Sci.* **28,** 93 (1990).
[18] P. R. LIN and R. C. BATRA, *Int. J. Engng. Sci.* **27,** 1155 (1989).
[19] R. JAYACHANDRAN and R. C. BATRA, *Int. J. Engng Sci.* **30,** 1009 (1992).
[20] M. E. BACKMAN and W. GOLDSMITH, *Int. J. Engng Sci.* **16,** 1 (1978).
[21] T. W. WRIGHT and K. FRANK, *SMIRT Symposium*, No. 14. Impact, Lausanne, Switzerland (1987).
[22] C. E. ANDERSON and S. R. BODNER, *Int. J. Impact Engng* **7,** 9 (1988).
[23] T. Z. BLAZYNSKI, *Materials at High Strain Rates* (Edited by T. Z. BLAZYNSKI). Elsevier Applied Science, London (1987).
[24] M. MACAULEY, *Introduction to Impact Engineering*. Chapman & Hall, London (1987).
[25] J. A. ZUKAS *et al.*, *Impact Dynamics*. Wiley–Interscience, New York (1982).
[26] J. A. ZUKAS (Ed.), *High Velocity Impact Dynamics*. Wiley–Interscience, New York (1990).
[27] G. BIRKHOFF, D. P. McDOUGALL, E. M. PUGH and G. TAYLOR, *Proc. Phys. Soc. Lond.* **57,** 147 (1945).
[28] D. C. PACK and W. M. EVANS, *Proc. Phys. Soc. Lond.* **B64,** 298 (1951).
[29] W. A. ALLEN and J. W. ROGERS, *J. Franklin Inst.* **272,** 275 (1961).
[30] V. P. ALEKSEEVSKII, *Comb. Expl. Shock Waves* **2,** 63 (1966). (Translation from Russian, Faraday Press, New York.)
[31] A. TATE, *J. Mech. Phys. Solids* **15,** 387 (1967).
[32] A. TATE, *J. Mech. Phys. Solids* **17,** 141 (1969).
[33] A. TATE, *Int. J. mech. Sci.* **28,** 535 (1986).
[34] A. TATE, *Int. J. mech. Sci.* **28,** 599 (1986).
[35] P. H. PIDSLEY, *J. Mech. Phys. Solids* **32,** 315 (1984).
[36] J. AWERBUCH, Technion–Israel Institute of Technology, MED Report No. 28 (1970).
[37] J. AWERBUCH and S. R. BODNER, *Int. J. Solids Struct.* **10,** 671 (1974).
[38] M. RAVID and S. R. BODNER, *Int. J. Engng Sci.* **21,** 577 (1983).
[39] M. RAVID, S. R. BODNER and I. HOLCMAN, *Int. J. Engng. Sci.* **25,** 473 (1987).
[40] M. J. FORRESTAL, K. OKAJIMA and V. K. LUK, *J. appl. Mech.* **55,** 755 (1988).
[41] R. C. BATRA and XINGJU CHEN, *Int. J. Engng. Sci.* **28,** 1347 (1990).
[42] X. CHEN and R. C. BATRA, *Acta mech.* **97,** 153 (1993).
[43] C. S. WHITE, C. A. BRONKHORST and L. ANAND, *Mech. Mater.* **10,** 127 (1990).
[44] Y. SHIMAZAKI and E. G. THOMPSON, *Int. J. numer Meth. Engng* **17,** 97 (1981).
[45] Y. M. WANG and R. C. BATRA, *Acta mech.* In press.

(Received 8 July 1992; accepted 25 August 1992)

stayed undeformed for all practical purposes. Here we take the penetrator to be rigid and give details of the deformation fields such as history of the temperature at a material point, history of the penetrator speed, and the distribution of the temperature and velocity field in the deforming target region. For the sixteen tests simulated herein, the computed depth of penetration has been found to match very well with that reported by Forrestal et al. [5].

We refer the reader to the review articles by Backman and Goldsmith [6], Wright and Frank [7], Anderson and Bodner [8], and the books by Zukas et al. [9], Blazynski [10], MaCauley [11], and Zukas [12] for a summary of the available literature on ballistic penetration. Awerbuch and Bodner [13], Ravid and Bodner [14], Ravid et al. [15], Forrestal et al. [16], and Batra and Chen [17] have proposed engineering models of different complexity in which a rigid penetrator impacts a deformable terget. Batra [18] has pointed out that the target deformations during the steady state phase of the penetration process are influenced strongly by the penetrator nose shape. He assumed the target/penetrator interface to be smooth. Here we also investigate the effect of the nose shape on transient deformations of the target and account for the effect of the frictional force at the interface. The shapes of the intensely deforming target material ahead of the penetrator nose for ellipsoidal and blunt nosed penetrators are quite different. In each case the plastic deformations of the target material are large enough to melt a thin layer of the target material adjoining the target/penetrator interface.

2 Formulation of the problem

In order to keep the paper self-contained we summarize below the pertinent equations. We presume that target deformations are axisymmetric, and use a fixed set of cylindrical coordinates with z-axis coincident with the axis of symmetry and pointing into the target and the origin at the top surface of the undeformed target to describe its deformations. The balance laws written in the referential description of motion and governing the thermomechanical deformations of the target are

$$(\varrho J) = 0, \tag{1.1}$$

$$\varrho_0 \dot{\boldsymbol{v}} = \text{Div } \boldsymbol{T}, \tag{1.2}$$

$$\varrho_0 \dot{e} = -\text{Div } \boldsymbol{Q} + tr\,(\boldsymbol{T}\dot{\boldsymbol{F}}^T), \tag{1.3}$$

where

$$J = \det \boldsymbol{F}, \quad \boldsymbol{F} = \text{Grad } \boldsymbol{x}, \tag{2}$$

$\boldsymbol{x}$ is the present position of a material particle that occupied place $\boldsymbol{X}$ in the reference configuration, ϱ its present mass density, ϱ_0 its mass density in the reference configuration, $\boldsymbol{v}$ the present velocity of a material particle, $\boldsymbol{T}$ the first Piola-Kirchhoff stress tensor, e the specific internal energy, $\boldsymbol{Q}$ the heat flux per unit reference area, a superimposed dot indicates the material time derivative, and operators Grad and Div signify the gradient and divergence of field quantities defined in the reference configuration. The balance laws (1.1)–(1.3) are supplemented by the following constitutive relations:

$$\boldsymbol{\sigma} = -p(\varrho)\,\mathbf{1} + 2\mu \boldsymbol{D}, \quad \boldsymbol{T} = \frac{\varrho_0}{\varrho}\,\boldsymbol{\sigma}(\boldsymbol{F}^{-1})^T, \tag{3.1, 2}$$

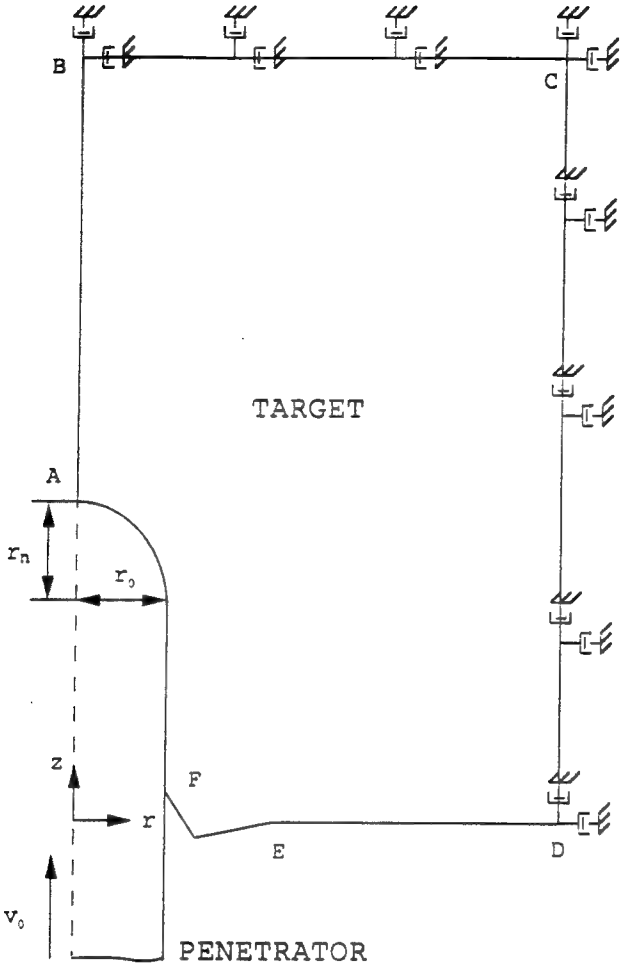

Fig. 1. A schematic sketch of the problem studied

z-direction, and we reckon time from the instant it impacts the top surface of the target at normal incidence.

In order to solve the problem numerically we analyze deformations of the finite target region ABCDEFA shown in Fig. 1 and impose the following boundary conditions on the bounding surfaces:

$$\boldsymbol{\sigma n} = \boldsymbol{0}, \quad \boldsymbol{q}\cdot\boldsymbol{n} = \boldsymbol{h}(\theta - \theta_a) \quad \text{on FED.} \tag{5.1, 2}$$

$$\sigma_{rz} = 0, \quad v_r = 0, \quad q_r = 0 \quad \text{on the axis of symmetry AB.} \tag{5.3-5}$$

$$\boldsymbol{q}\cdot\boldsymbol{n} = 0, \quad \boldsymbol{\sigma n} = \boldsymbol{0} \quad \text{at a point on AF where the penetrator surface is not in contact with the deforming target region.} \tag{5.6, 7}$$

$$\boldsymbol{q}\cdot\boldsymbol{n} = 0, \quad [\boldsymbol{v}\cdot\boldsymbol{n}] = 0, \quad \boldsymbol{e}_v\cdot\boldsymbol{\sigma n} = -f_s \quad \text{at points on AF where the penetrator and target surfaces are in contact with each other.} \tag{5.8-10}$$

$$f_n = -\varrho V_p v_n, \quad f_t = -\varrho V_s v_t, \quad \boldsymbol{q}\cdot\boldsymbol{n} = 0, \quad \text{on the bounding surface BCD.} \tag{5.11-13}$$

Here V_p and V_s are the speeds in the target material of the p-waves and s-waves, respectively, v_n and v_t are the normal and tangential components of the velocity of a target particle on the bounding surface BCD, and f_n and f_t equal, respectively, the normal and tangential forces exerted

values to other material parameters:

$$\varrho_0 = 2710\,\text{kg/m}^3, \quad A = 68.9\,\text{GPa}, \quad B = 0, \quad k = 120\,\text{Wm}^{-1}\,\text{C}^{-1},$$
$$c = 875\,\text{Jkg}^{-1}\,\text{C}^{-1}, \quad \theta_a = 22\,\text{C}, \quad h = 20\,\text{Wm}^{-2}\,\text{C}^{-1}, \quad \mu = 0.12, \quad \beta = 1.5. \tag{7.2}$$

According to our constitutive relations (3.2) and (3.3), when $\theta = 1$ (θ = melting temperature of the material, $\mu = 0$, the material behaves like an ideal fluid, and cannot support any shear stresses. In order to alleviate this problem, Eq. (3.3) was modified to

$$2\mu = \frac{\sigma_0}{\sqrt{3}\,I}\left(\frac{\dot{\psi}}{\psi_0}\right)^n (1 + bI)^m (1 - \nu\theta), \quad \theta \leqq 0.955\,\theta_m, \tag{8.1}$$

$$= \frac{0.045\sigma_0}{\sqrt{3}\,I}\left(\frac{\dot{\psi}}{\psi_0}\right)^n (1 + bI)^m, \quad \theta > 0.955\,\theta_m, \tag{8.2}$$

where θ_m equals the melting temperature of the target material. We note that the numerical simulations by Chen [3] of penetration tests involving conical-nosed penetrators, and the cavity expansion model of Forrestal et al. [5] do not consider thermal softening of the material. However, Chen and Batra [21] have shown that thermal softening influences strongly target's deformations.

3.1 *Results for a hemispherical-nosed penetrator*

Figure 2 exhibits the computed depth of penetration both with and without the consideration of frictional forces at the target penetrator interface, and the test values from Tables 1 and 2 of Forrestal et al. [5] for $r_0 = 2.54$ mm and 3.555 mm. The abscissa equals the non-dimensional number $\alpha = \varrho_t v_0^2/\sigma_0$ sometimes also referred to as the damage number [27]. Higher values of

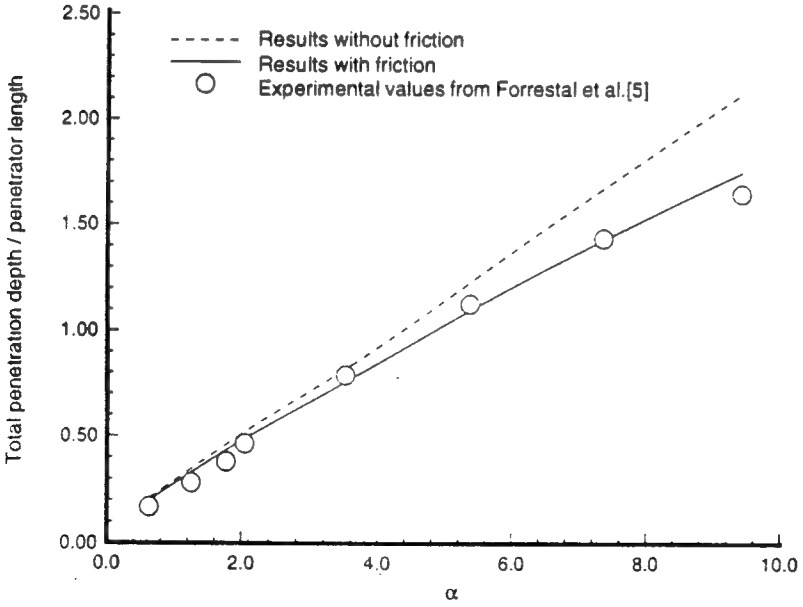

Fig. 2a

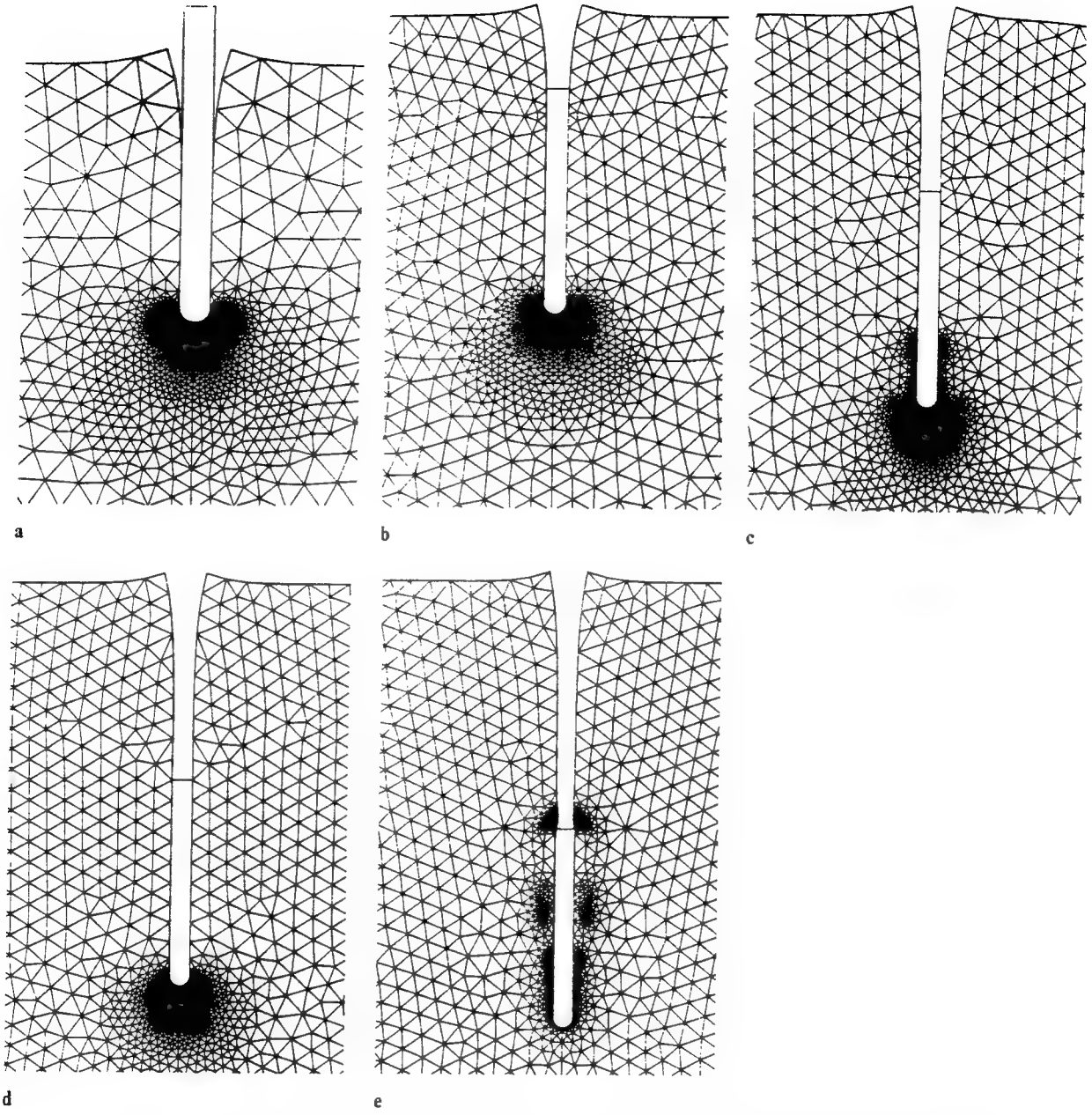

Fig. 3. Tunnel shapes with $\mu = 0.12$ when the penetrator speed has been reduced to **a** 0.796 9, **b** 0.605 0, and **c** 0.306 7 times the initial speed of 1.009 km s. Tunnel shapes at the end of the penetration process for $\mu = 0.12$ and 0.0 are given in **d** and **e** respectively

A comparison of these tunnel shapes with those reported in Figs. 5a–d of Chapter 3 of Chen's doctoral dissertation [28] suggests that for the case of a smooth target/penetrator interface more material on the sides of the interface is deformed severely as compared to that in the present case. When frictional effects are considered, the size of the severely deforming region ahead of the penetrator barely changes with time. This could be due to the retardation of the relative movement of the target material along the target/penetrator interface. Thus it will hinder

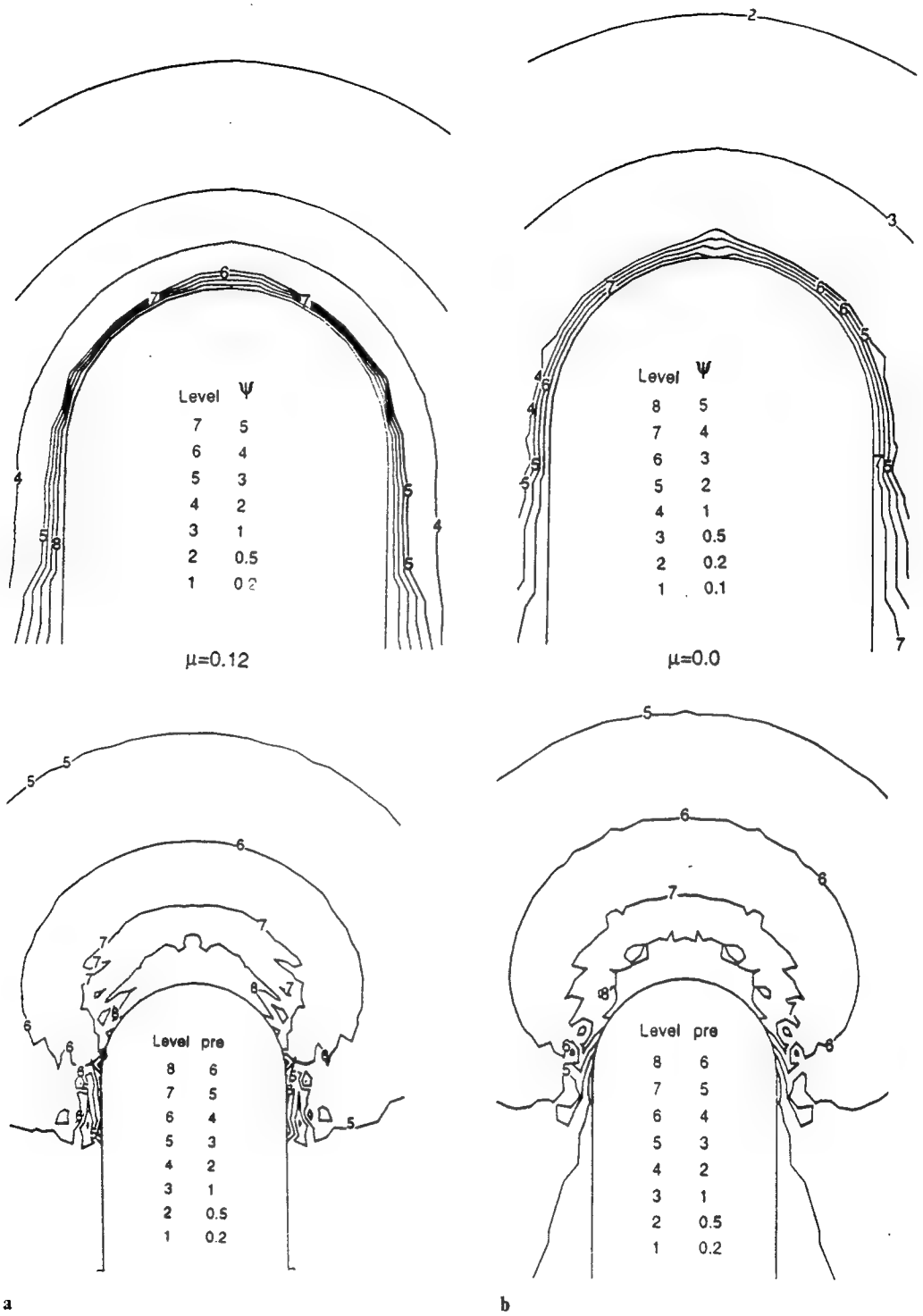

Fig. 5. Contours in the deforming target region of the hydrostatic pressure and the internal variable ψ when the penetrator speed has been reduced to 60% of the initial striking speed of 1.009 km s **a** with and **b** without frictional effects

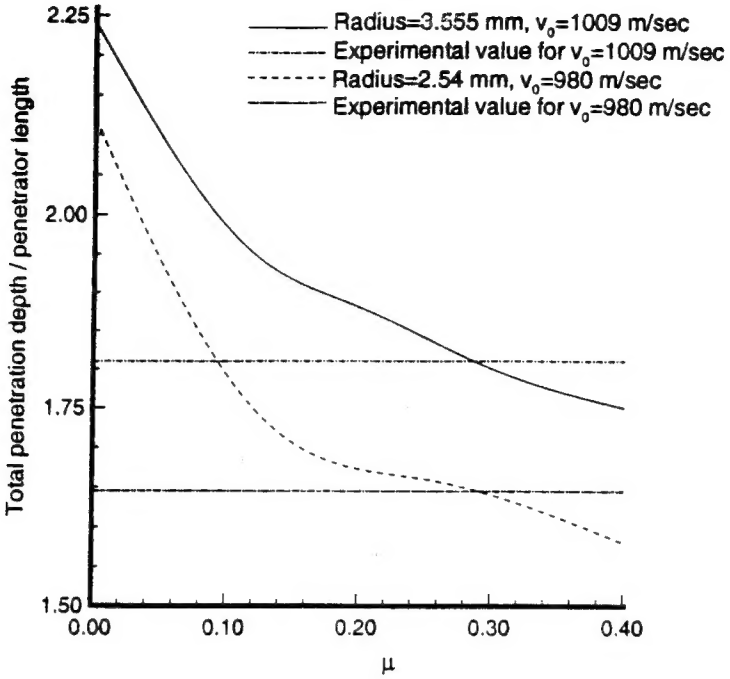

Fig. 7. Dependence of penetration depth upon μ for (i) penetrator radius = 3.555 mm, striking speed = 1.009 km/s (ii) penetrator radius = 2.54 mm, striking speed = 980 m/s

Figures 8 a, b depict respectively the time histories of the non-dimensional axial resisting force experienced by the penetrator, penetrator position and its speed for different values of μ. The axial resisting force is nondimensionalized by $\pi r_0^2 \sigma_0$, time by v_0/r_0, penetrator speed by v_0, and the penetrator position by its length. Here σ_0 equals the yield stress of the target material in a quasistatic simple compression test. In the beginning the resisting force is minimally affected by the value of μ. However, after about 10% of the duration of the penetration process, the resisting force gradually increases to about 10% higher than that computed without the consideration of the frictional force. This increase in the resting force is caused by the tangential traction exerted by the deforming target material on the penetrator surface. The normal traction on the target/penetrator interface is dominated by the hydrostatic pressure which is affected very little by the consideration of frictional forces. As expected, an increase in the value of μ increases the axial resisting force and thus decelerates the penetrator quicker. For the steady penetration problem, Chen and Batra [4] found that the axial resisting force depended moderately upon μ. The oscillations in the axial resisting force are probably due to high frequency oscillations resulting from multiple stress wave reflections from the top surface of the target. In our work we have not introduced any artificial viscosity to smoothen out these oscillations. The penetrator deceleration computed by Chen [3] also exhibited oscillatory behavior. However, the deceleration computed by differentiating twice with respect to time the penetrator position was found to be smoother than that computed directly from the numerical solution of the problem. For the case of the rough target/penetrator interface the penetrator speed decreases gradually to zero even towards the end of the penetration process. However, for smooth interface, the rate of decrease of the penetrator speed drops sharply towards the end of the penetration process. Because of the higher deceleration of the penetrator at larger values of μ, the total duration of the penetration process decreases as μ is increased.

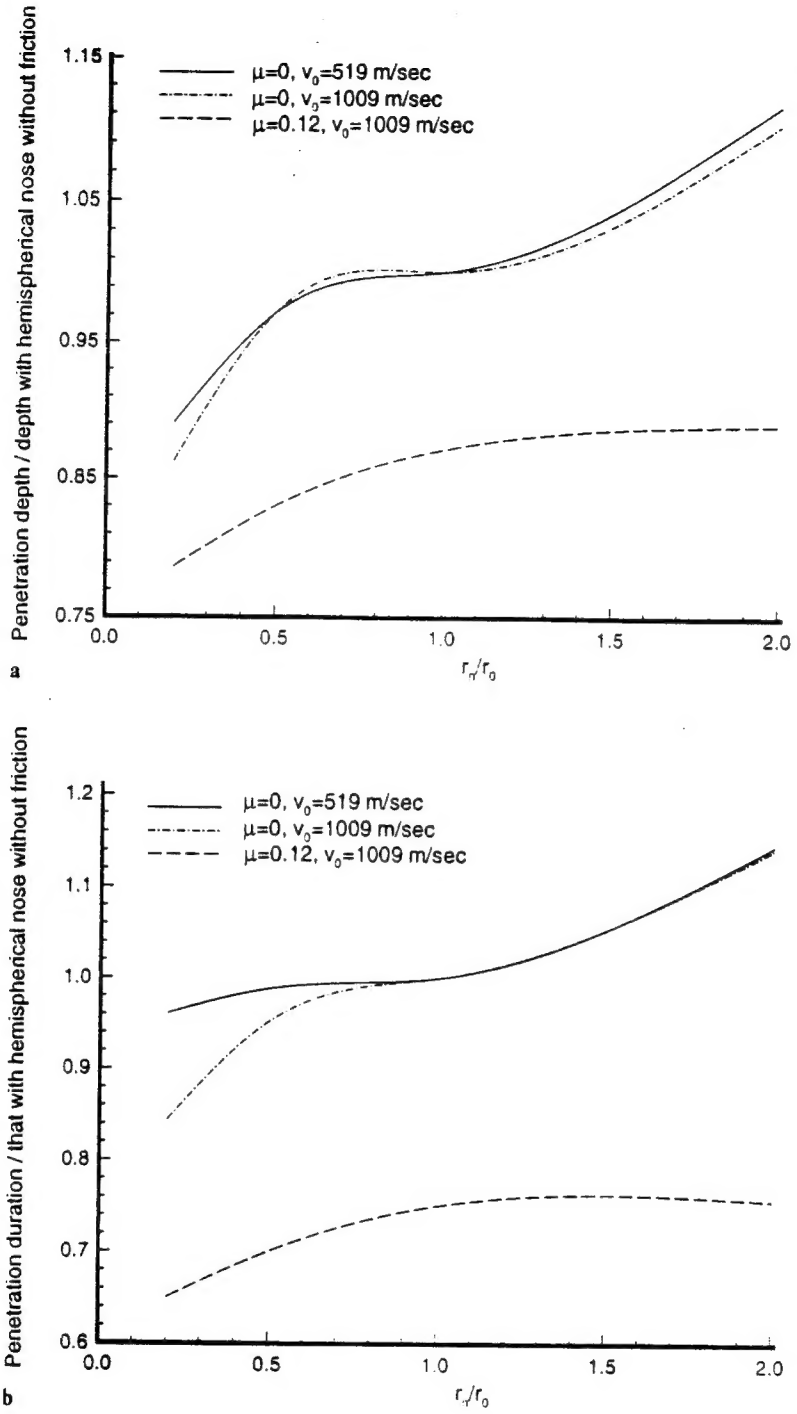

Fig. 9. Dependence upon r_n/r_0 of **a** the penetration depth and **b** the total duration of the penetration process for $\mu = 0$ and 0.12 at initial striking speed v_0 of 1.009 km s, and for $\mu = 0.0$ at $v_0 = 519\,m\,s$

Values of r_n/r_0 close to 0.2 imply a blunt nose, and those near 2 correspond to a moderately sharp nosed penetrator. In the plots of Fig. 9, the penetration time and the penetration depth are nondimensionalized with respect to their values for the smooth hemispherical nosed penetrator. For $\mu = 0$, the nose shape affects the normalized penetration depth and the duration of the

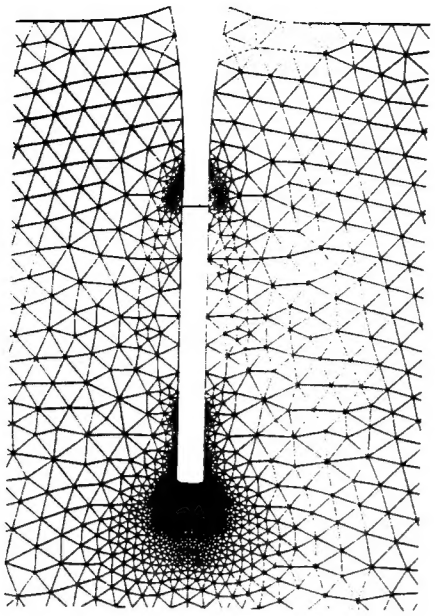

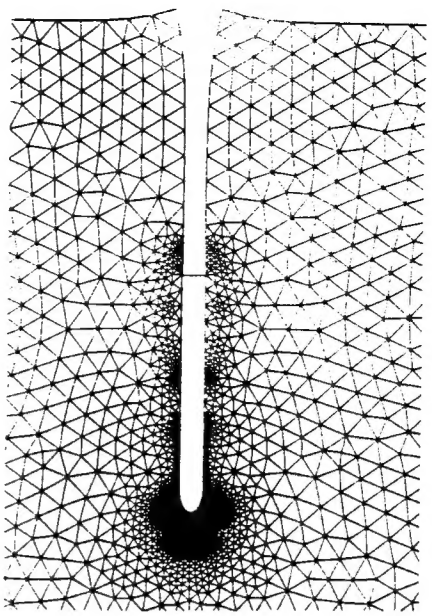

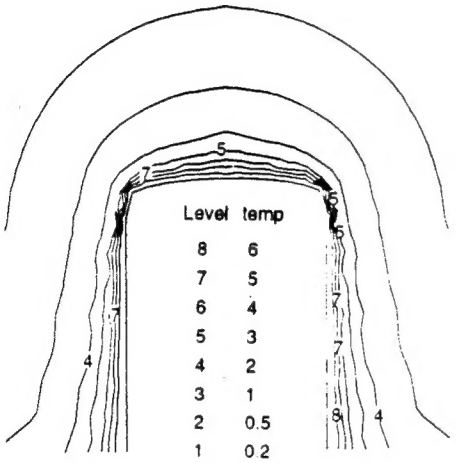
Level temp
8 6
7 5
6 4
5 3
4 2
3 1
2 0.5
1 0.2

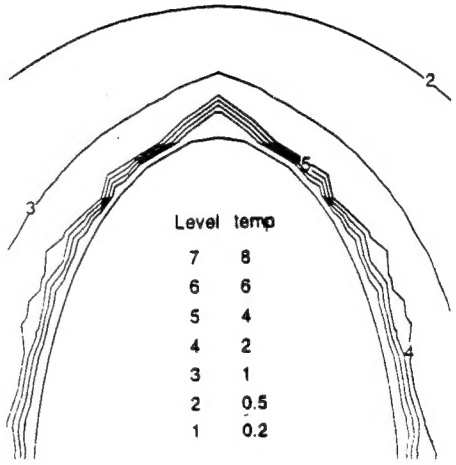
Level temp
7 8
6 6
5 4
4 2
3 1
2 0.5
1 0.2

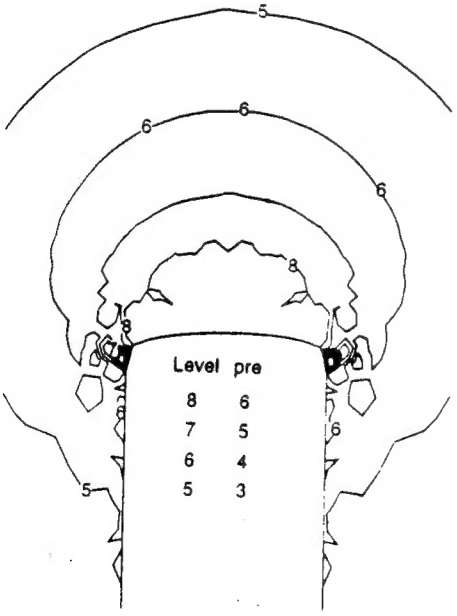
Level pre
8 6
7 5
6 4
5 3

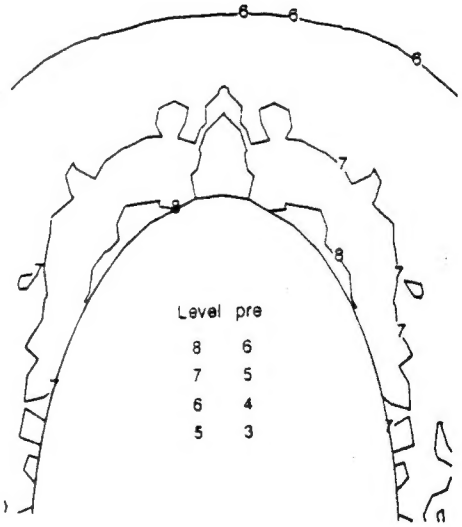
Level pre
8 6
7 5
6 4
5 3

periphery essentially equalled zero for each nose shape studied. The intense deformations of the target were found to spread deeper into the target for the blunt nosed penetrator as compared to other nose shapes which agrees with the presently computed results.

For many of the penetration problems studied herein a thin layer of the target material adjacent to the target/penetrator interface melted and thus underwent severe plastic deformations. However, ahead of the penetrator nose no thin intensely deforming regions, usually known as adiabatic shear bands, were observed. This is probably due to the fact that no failure criterion has been induded in the problem formulation and that the target has been taken to be very thick.

4 Conclusions

We have studied the dynamic thermomechanical deformations of a very thick thermally softening viscoplastic target impacted at normal incidence by a cylindrical rod. The frictional force on the target/penetrator interface has been modelled by a velocity dependent relation proposed earlier by Chen and Batra [4]. Results for different values of the coefficient of friction and penetrator nose shapes have been computed and presented. The computed depth of penetration has been found to agree very well with the test values reported by Forrestal et al. [5]. For the same striking speed the penetration depth increases rapidly when r_n/r_0 is increased from 0.2 to about 0.7 and from 1.2 to 2.0, but quite slowly for r_n/r_0 between 0.7 and 1.2. However, when frictional effects are neglected, higher values of r_n/r_0 result in greater values of the penetration depth. At an intermediate stage of the penetration process, more of the target material ahead of the penetrator and on its sides has been deformed severely for a blunt nosed penetrator as compared to that for penetrators with other nose shapes. In each case a thin layer of the target material adjoining the target penetrator interface essentially melted.

Acknowledgements

This work was supported by the U.S. Army Research Office Grant DAAL03-92-G-0315 to the University of Missouri-Rolla. Some of the computations were performed on the NSF sponsored supercomputer center at the University of Illinois in Urbana.

References

[1] Longcope, D. B., Forrestal, M. J.: Penetration of targets described by a Mohr-Coulomb failure criterion with a tension cutoff. J. Appl. Mech. **50**, 327 – 333 (1983).
[2] Forrestal, M. J.: Penetration into dry porous rock. Int. J. Solids Struct. **22**, 1485 – 1500 (1986).
[3] Chen, E. P.: Penetration into dry porous rock: a numerical study on sliding friction simulation. Theoret. and Appl. Fract. Mech. **11**, 135 – 141 (1989).
[4] Chen, X., Batra, R. C.: Effect of frictional force on the steady state axisymmetric deformations of a viscoplastic target. Acta Mech. **97**, 153 – 168 (1993).
[5] Forrestal, M. J., Brar, N. S., Luk, V. K.: Penetration of strain-hardening targets with rigid spherical-nosed rods. J. Appl. Mech. **58**, 7 – 10 (1991).
[6] Backman, M. E., Goldsmith, W.: The mechanics of penetration of projectiles into targets. Int. J. Eng. Sci. **16**, 1 – 99 (1978).
[7] Wright, T. W., Frank, K.: Approaches to penetration problems. In: Impact: effects of fast transient loading (Ammann, W. J., Lui, W. K., Studer, J. A., Zimmermann, T. eds.). Rotterdam: Balkema, A. A. 1988.